Three-Dimensional Au Microlattices as Positive Electrodes for Li−O_2 Batteries

Chen Xu,*,† Betar M. Gallant,‡ Phillip U. Wunderlich,§ Timm Lohmann,§ and Julia R. Greer†

†Division of Engineering and Applied Science, California Institute of Technology, Pasadena, California 91125, United States, ‡Division of Chemistry and Chemical Engineering, California Institute of Technology, Pasadena, California 91125, United States, and §Research and Technology Center, Robert Bosch LLC, Palo Alto, California 94304, United States

ABSTRACT We demonstrate the feasibility of using a 3-dimensional gold microlattice with a periodic porous structure and independently tunable surface composition as a Li−O_2 battery cathode. The structure provides a platform for studying electrochemical reactions in architected Li−O_2 electrodes with large (300 μm) pore sizes. The lack of carbon and chemical binders in these Au microlattices enabled the investigation of chemical and morphological processes that occur on the surfaces of the microlattice during cycling. Li−O_2 cells with Au microlattice cathodes were discharged in 0.5 M lithium-bis(trifluoromethane)sulfonamide (LiTFSI) in a 1,2-dimethoxyethane (DME) electrolyte, with lithium metal foil as the anode. SEM analysis of microlattice cathodes after first discharge revealed the presence of toroidal-shaped 500−700 nm particles covering the surface of the electrode, which disappeared upon subsequent charging. Raman and FTIR spectroscopy analysis determined these particulates to be Li_2O_2. The morphology of discharge products evolved with cycling into micrometer-sized clusters of arranged "platelets", with a higher amount of side reaction products such as Li_2CO_3 and LiOH. This work shows that properly designed 3-dimensional architected materials may provide a useful foundation for investigating fundamental surface electrochemistry while simultaneously enabling mechanical robustness and enhancing the surface area over a factor of 30 compared with a thin film with the same foot print.

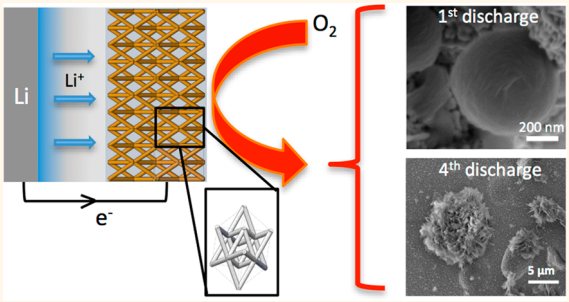

KEYWORDS: Li−O_2 battery · microlattice · polycrystalline Au · toroids

Rechargeable Li−O_2 batteries have been the subject of significant research efforts because of their potential as efficient energy storage devices in electric vehicles. A "practical" Li−O_2 cell may have a gravimetric specific energy 2 to 5 times higher than that of the current state-of-the-art Li-ion battery,[1,2] allowing a vehicle powered by this device to travel more than 300 miles between charges.[3] Among many challenges, a lack of chemical stability of the positive electrode material,[4−6] along with poor catalytic activity toward oxygen reduction reaction (ORR and OER),[3] remain key obstacles that prevent the utilization of Li−O_2 batteries in commercial applications. Initial investigations[5,7−9] utilized mostly carbon-based positive electrodes because of their low cost and weight, high electrical conductivity, high surface areas, and structural versatility. Oxidation of carbon upon contact with Li_2O_2 and/or battery operation in a highly oxidizing environment during charge[4−6,10] has been proposed to explain the widely observed coformation of Li_2CO_3, which accumulates with cycling and causes rapid degradation in performance. Select oxides,[11] carbides,[12] and noble metals[13] can significantly improve the chemical stability against oxidation when compared to carbon. For example, Thotiyl *et al.*[12] found that in cells using dimethyl sulfoxide (DMSO) as electrolyte solvent, a TiC nanoparticle cathode produced 40 times less Li_2CO_3 at the end of the fifth discharge compared to a carbon electrode, which ultimately led to 98% capacity retention after 100 cycles. Nanoporous Au foils have also been reported as chemically stable electrodes capable of high cyclability.[13] The discharge product morphology for these reportedly stable electrode materials has not been systematically investigated, which is critical for developing design principles for using these materials as structured electrodes.

Early efforts in this area focused on electrode structure design to maximize useable

* Address correspondence to chenxu@caltech.edu.

Received for review January 21, 2015 and accepted May 7, 2015.

Published online May 07, 2015
10.1021/acsnano.5b00443

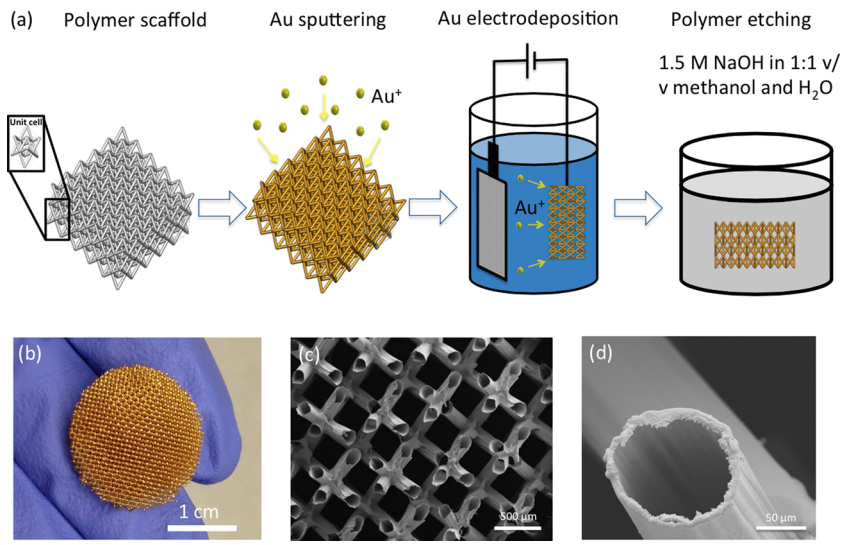

Figure 1. (a) Schematic of the step-by-step fabrication process of hollow Au microlattices. (b) Optical image of Au microlattice cathode, with a diameter of 17 mm and a height of 3 mm. (c) A top down SEM image of a Au microlattice, with exposed and hollowed out beams in the field of view. (d) SEM image of an individual beam showing the hollow interior.

pore volume and to minimize O_2 transport losses. Chemical stability issues ultimately delayed progress in this area, which shifted the attention toward identifying stable electrode−electrolyte configurations.[9,12−17] As a result, recent efforts have been focused on understanding electrochemical processes using rotating disk electrode (RDE), which permit minimization of O_2 transport losses and monitoring of kinetically controlled electrochemical processes. RDE experiments require beaker cell setups with excess electrolyte, rendering investigation of electrolyte decomposition challenging. Morphological and chemical characterization of discharged disk electrodes in such setups is also challenging, and extrapolation to structured electrodes with porosity is not straightforward.

Microlattices are cellular materials with a periodic structure and a tunable density to as low as 0.9 kg m^{-3}.[18] The typical unit cell size ranges from hundreds of micrometers to a few millimeters. Some microlattices, called microtrusses, have been investigated for a wide range of applications such as thermal insulation, shock or vibration damping, and acoustic absorption.[18] The macroscopic well-structured pores make these materials potentially useful as positive electrodes in Li−O_2 batteries because they could, in principle, accommodate large amounts of discharge product while minimizing transport losses. Their three-dimensional architecture yields a true surface area up to 30 times that of its projected flat footprint, which provides access to much lower surface area-normalized discharge currents. The versatility of microlattice fabrication lends itself to producing a variety of low-density materials like Ni−P alloys and metallic glasses, metals (Cu), and ceramics (SiO_2), which invokes the unique advantage of RDE experiments, which is the ability to change the electrode material without influencing electrode structure or transport.[19] This ability to rationally tune surface composition independently from electrode structure can permit fundamental, well-controlled surface studies of the intrinsic activity differences of different electrode materials toward ORR/OER. Microlattices can be assembled in closed Li−O_2 cells with more realistic electrolyte quantities than in beaker cells, allowing investigation of chemical stability and morphological evolution during electrode cycling.

In this work, we use Au as the prototype electrode material because of its chemical stability and DME as the electrolyte because of its high yield of Li_2O_2 upon first discharge.[10] We observed the formation of Li_2O_2 toroids with 500−700 nm diameter on the surface of the microlattice at a low discharge rate of 70 nA cm^{-2}_{true} (current density normalized over electrochemically active surface area, hereon denoted "true" surface area); no toroids were observed when discharge rates were higher, 210 nA cm^{-2}_{true}. The morphology of the discharge product evolved during cycling, and by the fourth discharge, it was comprised of clusters of platelets with the cluster size ranging from 5−10 μm in diameter. The mechanical robustness of the microlattice allowed it to retain its integrity during testing, and the large pore size permitted investigation of the morphology and composition of the discharge products using SEM, Raman, and FTIR spectroscopic analysis.

RESULTS AND DISCUSSION

Fabrication of Hollow Au Microlattices. The fabrication procedure of the microlattices is shown in Figure 1(a). Step 1 shows the fabrication of a 3-dimensional polymer scaffold by exposing a 2-dimensional mask with a pattern of circular apertures over a thiolene based photomonomer. Within the photomonomer, self-propagating photopolymer waveguides originate at each

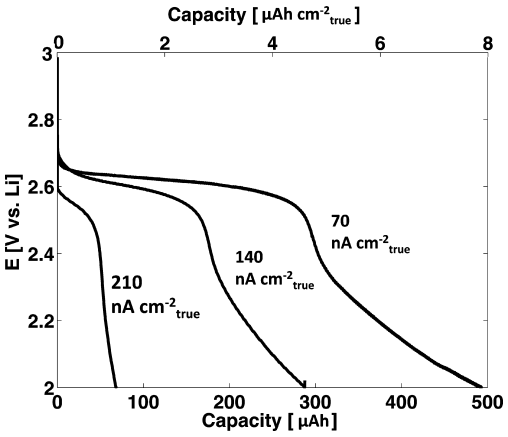

Figure 2. First discharge of Au microlattice positive electrodes over a range of true surface area-normalized currents.

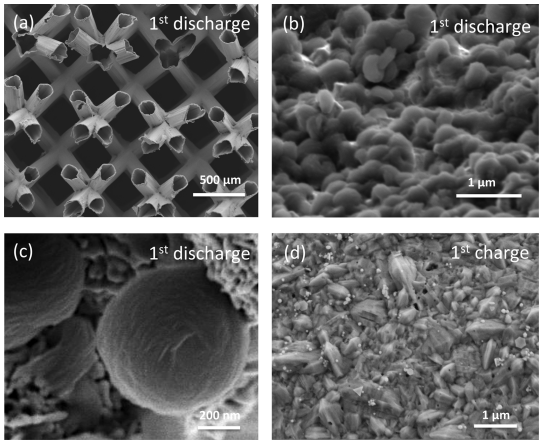

Figure 3. SEM images of (a−c) the surface of a microlattice after the first discharge at 70 nA cm^2_{true}, with different magnifications and (d) the surface of a microlattice after the first charge at 70 nA cm^2_{true}.

aperture in the direction of the UV collimated beam and polymerize, forming an interconnected solid structure.[20] The octahedral geometry of the unit cell originates directly from this exposure method and is thus intrinsically linked to the fabrication method. The minimum feature size of 100 μm for the diameter of the individual beams is imposed by the UV light diffraction limit within the thiolene based photomonomer. Next, a seed layer of Au is sputtered onto the polymer scaffold, on which ~5 μm of Au is further electrodeposited to allow the structure be mechanically robust enough to maintain its original geometry upon cell assembly and disassembly. The true surface area of the fabricated microlattice cathode was determined by cyclic voltammetry (CV) using standard practices adapted from metal electrocatalyst surface area measurements.[21−23]

Rate Capability and Cycling Tests. The galvanostatic discharge behavior of Au microlattices is shown in Figure 2. A discharge voltage plateau is observed at 2.6 V at 70 nA cm^{-2}_{true}, which decreased to 2.5 V as the rate increased to 210 nA cm^{-2}_{true}. A sharp decrease in voltage occurs toward the end of the discharge, immediately followed by a more gradual slope until the potential reaches 2 V. Further tests are needed to probe the origin of this sloping profile, which could potentially result from ohmic limitations through the deposited films. In previous reports on nanoporous Au in DMSO, Peng *et al.*[13] observed a discharge voltage around 2.5 V, with a capacity of 0.6 μAh cm^{-2}_{true} at the discharge rate of 1.0 μA cm^{-2}_{true}. The highest rate of 210 nA cm^{-2}_{true} used in this work was significantly lower than that reported previously and yielded a capacity of 1.0 μAh cm^{-2}_{true}; the lowest rate of 70 nA cm^{-2}_{true} yielded a discharge capacity of 7.0 μAh cm^{-2}_{true}. The relatively low specific surface area of ~140 $cm^2\ g^{-1}$ offered by these Au microlattices causes the true surface-area normalized capacities to be significantly higher than those in literature, which enables the investigation of the product chemistry and morphology for more practical discharge capacities.

SEM images of the microlattice electrode after first discharge are shown in Figure 3(a) and reveal that the sample retained its shape integrity during testing, which can be attributed to the favorable mechanical properties of microlattices.[18,24] Figure 3(b,c) shows SEM images of the surface of a microlattice discharged at 70 nA cm^{-2}_{true}, which is populated with densely spaced toroidal-shaped particles averaging 500 nm in diameter. The size and morphology of these particles are consistent with the Li_2O_2 particles found on carbon-based cathodes with[2,8] and without[6,8,25] catalysts, and on TiC[12] over a range of electrolytes including DME and DMSO. No prior literature has reported the observation of toroidal Li_2O_2 particles on pure Au surfaces with no carbon present. These findings suggest that the electrochemical and chemical processes that lead to the formation of toroids, and their subsequent growth, are not limited to carbon. The electrodes discharged at a higher rate of 210 nA cm^{-2}_{true} (Figure S3) did not contain toroidal particles, consistent with prior reports on carbon electrodes[25−27] in which toroidal particles were observed only at relatively low, near-thermodynamic, currents. Recent publications suggested that Li_2O_2 toroid growth is also influenced by water concentration within the electrolyte. Aetukuri *et al.*[28] proposed that Li_2O_2 toroidal crystallites are formed *via* a solution-mediated electrochemical process driven by LiO_2 partial solubility in the presence of H_2O, without which only Li_2O_2 thin films is formed, regardless of current density. Schwenke *et al.*[29] systematically investigated the influence of water content and true surface area current density on discharge product morphology. Specifically, the authors observed formation of toroids 400 nm in diameter on carbon paper electrodes discharged at 16 nA cm^{-2}_{true}, with electrolyte H_2O content of 1000 ppm; when current is increased to 480 nA cm^{-2}_{true}, the precipitate takes the form of a film densely covering the surface of the electrode. This trend roughly agrees with our observations

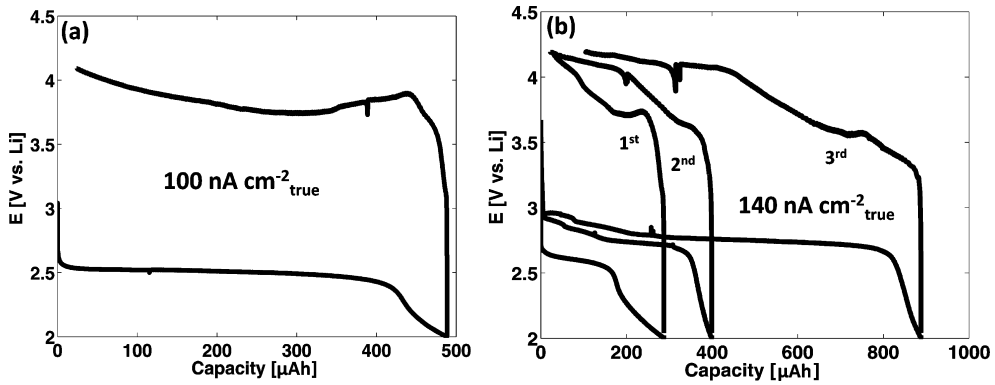

Figure 4. Electrochemical data of (a) first cycle at 100 nA cm^{2}_{true} and (b) first 3 cycles at 140 nA cm^{2}_{true}.

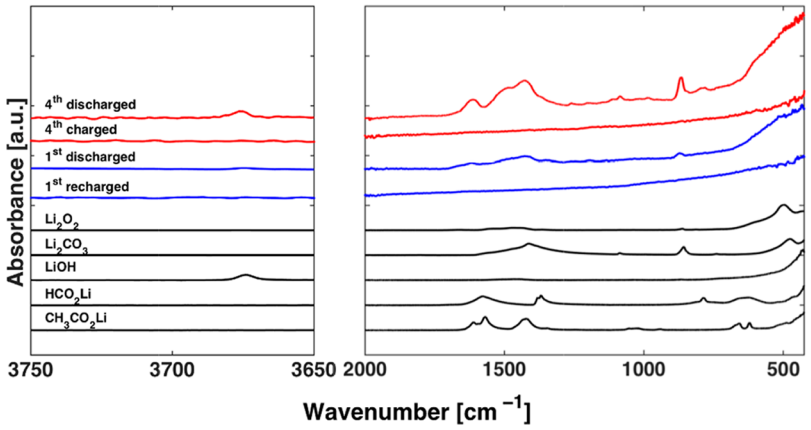

Figure 5. FTIR spectra of discharged, charged and cycled microlattice electrode.

of toroid formation at 70 nA cm^{-2}_{true} and lack of toroids at 210 nA cm^{-2}_{true}, and while the water concentration of our electrolyte during operation is unknown, it is plausible that continuous moisture contamination may have taken place during our low current tests, which typically takes days. Investigations of possible moisture contamination are given in the next section. Figure 3(d) shows the surface of a microlattice after the first charge. The visible roughness corresponds to the polycrystalline nature of the electrodeposited Au film, consistent with the surface texture of pristine microlattices shown in Figure S1.

Figure 4(a,b) shows the first galvanostatic cycle at 100 nA cm^{-2}_{true} and the first three cycles at 140 nA cm^{-2}_{true}, respectively, for two different truss electrodes tested with a lower cutoff voltage of 2 V and an upper cutoff voltage of 4.1 V *vs* Li. During charging the potential quickly rose to 3.9 V, after which it dropped down to 3.75 V at 40% of the total charge capacity (Figure 4(a)). The voltage then rose gradually to 4.1 V. Following the first charge, SEM images (Figure 2(d)) revealed the regeneration of a clean microlattice surface, with the nearly complete removal of toroidal particles. Some particles under 100 nm in diameter, most likely LiTFSI salt, remained whose total amount was insufficient to generate signals in FTIR or EDS. With cycling, however, both the discharge and charge capacities increased considerably, as shown in Figure 4(b). For example, the discharge capacities increased with each cycle, from 288 μAh in the first cycle to 399 μAh in the second and 888 μAh in the third, while the discharge potential also rose, from the original 2.60 to 2.75 V during the third discharge. The increase in capacity during cycling was observed previously in studies using ether solvents[30] and glyme solvents.[31] This work concluded that the higher measured capacity was a result of solvent oxidation caused by high charging potential; the capacity measured after the first discharge was 3 times higher than that of cells with fresh electrolyte. In another study,[32] an increase in discharge potential was observed in the cells that suffered moisture contamination, which can be related to the higher reversible potential for LiOH formation (3.35 V *vs* Li) compared to Li_2O_2 (2.96 V *vs* Li).

FTIR spectroscopy were used to investigate the composition of the reaction products and revealed significant chemical changes as a function of cycle number. Figure 5 shows the IR spectra for electrodes after the first discharge and charge, fourth discharge and charge, along with the powder reference spectra for Li_2CO_3, HCO_2Li, CH_3CO_2Li and LiOH. Li_2O_2 is found to be the predominant discharge product as indicated by the broad peak at 500 cm^{-1}, accompanied by several peaks centered at 1400 and 860 cm^{-1}, which

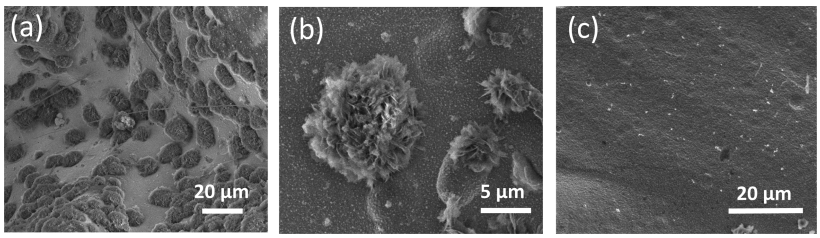

Figure 6. SEM images of a microlattice after (a,b) fourth discharge and (c) fourth charge.

suggests the presence of small amount of Li_2CO_3. The Raman spectra given in Figure S5 supports this claim, where a peak at 790 cm^{-1} indicates the presence of Li_2O_2; a lack of peak attributed to Li_2CO_3 may be due to the small amount of carbonate present, and also the relative Raman inactivity of the C−O bond.[33,34] To determine whether the origin of Li_2CO_3 comes from atmospheric CO_2 during post characterization or from the testing of the cell, we collected a spectrum of a discharged cathode in a N_2 glovebox (Figure S4, Supporting Information). The detection range of this setup is limited to a range of 4000 to 600 cm^{-1} (Nicolet iS5, ThermoScientific, Inc.), suitable for Li_2CO_3 detection but not Li_2O_2 whose peak onset is at 675 cm^{-1}. The measured spectrum clearly reveals the presence of Li_2CO_3 (Figure S3), which indicates that it did not form as a result of exposure to atmosphere during postcharacterization. These results do not conclusively answer whether Li_2CO_3 formed electrochemically or chemically, *i.e.*, by potential leakage during cell testing, which is the subject of ongoing study. The formation of Li_2CO_3 after the first discharge, along with HCO_2Li or CH_3CO_2Li as indicated by the IR peaks at 1600 cm^{-1}, agrees with observations by Peng *et al.*[13] using DMSO and a nanoporous Au electrode: peaks associated with Li_2CO_3, HCO_2Li and CH_3CO_2Li were observed after the first discharge, with their amounts comprising less than 1% of the total discharge product. These authors also found that the side reaction products were consistently oxidized during charge, a finding reproduced in this work where the IR data showed no peaks associated with any of the above-mentioned products after the first and fourth charge. We observed substantial accumulation of Li_2CO_3, HCO_2Li and CH_3CO_2Li after the fourth discharge. LiOH was also detected within the electrode after cycling, as indicated by the peak at 3675 cm^{-1}. The presence of LiOH in the electrode after cycling could stem from the incorporation or electrochemical generation of water with prolonged testing, which is in agreement with changes in the discharge voltage and capacity during cycling (Figure 4).[32,35] A direct generation of LiOH as an electrochemical discharge product has also been proposed.[36,37] Ongoing efforts are dedicated to investigating the origin of the formed LiOH.

SEM images of cycled microlattice electrodes reveal a corresponding change in discharge product morphology with cycling. Figure 6(a,b) shows the surface of the microlattice following the fourth discharge, at different magnifications. Clusters of "platelets" with cluster diameters between 5−10 μm were observed. Such Li_2O_2 "platelet" morphologies have been observed before on nanoporous gold (NPG) discharged in LiTFSI with dimethysulfoxide (DMSO) as electrolyte,[38] and as freely distributed "platelets" on α-MnO_2 nanowires discharged in $LiCF_3SO_3$ with tetraethylene glycol dimethyl ether (TEGDME) as electrolyte.[39] The closest resemblance to our structures comes from discharge products formed on a 3-dimensional Ni-Co_2O_4 nanowire array/carbon cloth cathode (carbon cloth acting as a template for the growth of the nanowire array)[40] discharged in LiTFSI with DME as electrolyte. That study observed "porous ball" shaped discharge products, with diameters ranging from hundreds of nanometers to a several micrometers. Selected area electron diffraction (SAED) of those particles confirmed that the products consisted of nanocrystalline Li_2O_2. The spectroscopy results in this work indicate that these structures represent a combination of Li_2O_2, Li_2CO_3, HCO_2Li and CH_3CO_2Li. Figure 6(c) shows the surface after the fourth charge. We find a surface devoid of discharge products with the morphologies shown in Figure 6(a,b).

CONCLUSIONS

We demonstrated the feasibility of using a 3-D architected microlattice as a positive electrode for Li−O_2 batteries. Using Au as the electrode material and DME as the electrolyte solvent, we observed the formation of toroidal-shaped Li_2O_2 as the predominant product after first discharge, their complete removal upon charge, and the accumulation of Li_2CO_3, HCO_2Li and CH_3CO_2Li after multiple cycles. These findings demonstrate that 3-dimensional architected materials provide a useful testbed when serving as electrodes for studying fundamental electrochemistry and discharge product morphology. Optimization of the geometry, unit cell size and the electrode surface material used in the microlattices, while beyond the scope of this work, could be achieved using alternative versatile fabrication methods, for example, 2-photon lithography,[44] microstereolithography,[42] interferometric lithography,[43] or template directed electrodeposition.[41] In general, optimally structured meta-materials for Li−O_2 electrodes

will likely reflect a balance between several design constraints. These include the need for large pore volumes for mass transport (O_2 and possible discharge intermediate diffusion) and accommodation of discharge product, as well as maximum total electrode surface areas to sustain high-rate discharge or charge reactions with minimal overpotentials. The ability to decouple the microscale pore structure from the selection of surface composition and area, for example, through manipulation of the coating process and surface roughness, therefore represents a new direction in electrode design for metal-air systems. Future work studying Li$-O_2$ chemistry on different material surfaces while preserving the electrode geometry and mechanical integrity will provide insight on optimizing the chemical stability and catalytic activity of electrode materials toward ORR/OER.

METHODS

Fabrication of Hollow Au Microlattices. 100 nm of Au is sputtered onto the polymer scaffold in an Ar atmosphere (AJA International ATC Orion sputterer, DC current source, 56 W) with a gas flow rate of 10 sccm, maintaining a working pressure of 3 mTorr.[41] To ultimately obtain a sufficiently stiff hollow structure that can survive handling and maintain its integrity throughout cell testing, an additional ~5 μm of Au (TSG-250, Transene) was electrodeposited onto the initial 100 nm-thick sputtered layer of Au. The plating temperature was maintained at 60 °C, and the solution was stirred with a magnetic stir bar to maintain optimum flux to the surface. The current density was maintained at ~1 mA cm^{-2}. The surface area used to normalize the deposition current was estimated by modeling the microtruss in CAD, with the unit cell dimensions used as input parameters. Following electrodeposition, the coated microlattices were cut into "pucks" roughly 3 mm in height and 17 mm in diameter. The incisions made during this process exposed the polymer within the interior of the truss to the etching solution (1.5 M NaOH, in 1:1 v/v methanol and DI water) used to dissolve the polymer. Etching was performed for 24 h at 40 °C,[24] after which the sample was thoroughly cleaned in DI water. The resulting structure, shown in Figure 1(b,d), is a 3-dimensional octahedral network comprised of hollow, 5 μm-thick Au tubes. SEM images in Figure 1 reveal that the pore size was roughly 300 μm, the diameter of the individual tubes was 150 μm, and the coating was relatively uniform, with a thickness of 5 μm.

Characterization. SEM images were obtained in the FEI Versa 3D DualBeam Scanning Electron Microscope (SEM) under high vacuum mode with an acceleration voltage of 5 kV. FTIR spectra were measured on a Nicolet 860 Magna spectrometer with a Durascope attenuated total reflectance (ATR) unit and a KBr window to enhance the signal-to-noise detection in the range of 400−4000 cm^{-1}. Raman spectroscopy was performed on a Renishaw M1000 Micro Raman Spectrometer System, utilizing an Ar ion laser at 514.5 nm. Both the FTIR and Raman instruments operate in air. Scans were usually kept under 5 min. Another FTIR instrument (Nicolet iS5), with a detection window of 600−4000 cm^{-1}, located in a glovebox, was used to probe whether the lithium carbonate peaks detected in open air measurements came from atmospheric contamination or from electrolyte decomposition. Pristine Au microlattices do not have any Raman or IR peaks in the wavenumber range of interest; their spectra are not shown in the figures. Reference spectra of expected discharge products are taken from commercial powders (assay >99.0%, Sigma-Aldrich).

Cell Assembly and Electrochemical Measurements. Cell assembly and electrochemical testing were performed at Bosch Research and Technology Center (RTC) at Palo Alto, CA. Electrodes were held at 120 °C under a vacuum for 12 h in an oven/antechamber connected to an Ar glovebox (MBraun, H_2O < 0.1 ppm, O_2 < 0.1 ppm), before being transferred directly into the glovebox without exposure to the ambient. The electrochemical cells were commercially available (EL-CELL GmbH, Germany). Assembled Li$-O_2$ cells comprised a Li metal anode, electrolyte-impregnated separator (0.5 M LiTFSI in DME contained in binder-free borosilicate glass, 260 μm thick), and microlattice cathode. DME (anhydrous, water content 10−30 ppm, Sigma-Aldrich) was dried for several days over molecular sieves in the Ar glovebox. After assembly, the sealed cells were transferred out of the glovebox to be connected to an O_2 channel (Teflon) and purged. The gas connection and purging process were carefully controlled to minimize atmospheric contamination by blanketing the cell ports with dry O_2 and maintaining a positive pressure of O_2 within the cell during purging, with an ultimate cell pressure maintained at 25 psi. Cells were then subjected to a rest step at open circuit in O_2 for 10 h to stabilize open circuit voltage (OCV) before discharge (the typical OCV was ~3.0 V *vs* Li). Electrochemical testing was performed using an Arbin BT2000 battery test setup. After testing, cells were opened and dissembled in an Ar glovebox, washed in DME, and vacuum-dried at room temperature for a minimum of 30 min in the antechamber of the glovebox. Samples were then placed back into the glovebox with no air exposure and placed into high-density polyethylene (HDPE) bottles (Nalgene, Sigma-Aldrich) that were heat sealed in airtight foil bags (Sigma-Aldrich) for subsequent transfer and characterization.

Determination of True Surface Area. Microlattice electrodes were tested in a three-electrode beaker cell, with a Ag/AgCl reference electrode and Pt mesh counter electrode. CVs were conducted in the potential range of 0.4 to 1.4 V *vs* Ag/AgCl in 0.5 M H_2SO_4 at a scan rate of 50 mV s^{-1}. The first ~15 initial cycles were used to stabilize the CV curves, after which the CV for surface area measurement was performed. A typical voltamogramm is shown in Figure S1(a) (Supporting Information). The anodic peaks at 1.15 and 1.3 V *vs* Ag/AgCl correspond to the formation of Au surface oxides, and the cathodic peak at 0.9 V arises from corresponding reduction.[22] Using charge integration under the reduction peak while subtracting contributions from double layer capacitance, the total surface area was obtained by dividing the integrated value by the charge per surface area of Au (400 μC cm^{-2}), as adapted from literature.[22,23] The experimentally measured value of ~140 cm^2 g^{-1} were only 15% higher than that predicted by CAD software. The slightly higher surface area measured electrochemically likely stems from the roughness of the Au surface caused by the polycrystalline microstructure, as well as the initial roughness of the polymer. Figure S1(b) shows SEM image of the pristine Au microlattice surface with crystallites up to 500 nm. The XRD spectrum shown in Figure S2 confirms the polycrystalline nature of the deposited gold. Such a low specific surface area of 140 cm^2 g^{-1} arises from the 5 μm-thick Au coating, which is necessary to retain suitable mechanical stiffness and strength and the relatively smooth surface of the structure.

Conflict of Interest: The authors declare no competing financial interest.

Acknowledgment. This work is supported by the Bosch Energy Research Network (BERN). The authors gratefully acknowledge Kavli Nanoscience Institute at Caltech, Dr. Jake Christensen of Robert Bosch, LLC for fruitful discussions, and Prof. George Rossman of Caltech for his help with Raman and FTIR measurements.

Supporting Information Available: Cyclic voltamogramm and SEM image of as-fabricated Au microlattice, XRD pattern of as-fabricated Au microlattice, SEM image of the surface of a Au microlattice discharged at a higher rate of 210 nA cm$^{-2}_{true}$, FTIR spectra of a discharged electrode taken inside a glovebox

without exposure to atmosphere, Raman spetra of electrodes after the first discharge, first charge and fourth discharge. The Supporting Information is available free of charge on the ACS Publications website at DOI: 10.1021/acsnano.5b00443.

REFERENCES AND NOTES

1. Christensen, J.; Albertus, P.; Sanchez-Carrera, R. S.; Lohmann, T.; Kozinsky, B.; Liedtke, R.; Ahmed, J.; Kojic, A. A Critical Review of Li/Air Batteries. *J. Electrochem. Soc.* **2012**, *159*, R1.
2. Lu, Y.-C.; Gallant, B. M.; Kwabi, D. G.; Harding, J. R.; Mitchell, R. R.; Whittingham, M. S.; Shao-Horn, Y. Lithium−Oxygen Batteries: Bridging Mechanistic Understanding and Battery Performance. *Energy Environ. Sci.* **2013**, *6*, 750.
3. Bruce, P. G.; Freunberger, S. A. Li−O_2 and Li-S Batteries with High Energy Storage. *Nat. Mater.* **2012**, *11*, 19–30.
4. Ottakam Thotiyl, M. M.; Freunberger, S. a; Peng, Z.; Bruce, P. G. The Carbon Electrode in Nonaqueous Li−O_2 Cells. *J. Am. Chem. Soc.* **2013**, *135*, 494–500.
5. McCloskey, B. D.; Speidel, A.; Scheffler, R.; Miller, D. C.; Viswanathan, V.; Hummelshøj, J. S.; Nørskov, J. K.; Luntz, A. C. Twin Problems of Interfacial Carbonate Formation in Nonaqueous Li−O_2 Batteries. *J. Phys. Chem. Lett.* **2012**, *3*, 997–1001.
6. Gallant, B. M.; Mitchell, R. R.; Kwabi, D. G.; Zhou, J.; Zuin, L.; Thompson, C. V.; Shao-Horn, Y. Chemical and Morphological Changes of Li−O_2 Battery Electrodes upon Cycling. *J. Phys. Chem. C* **2012**, *116*, 20800–20805.
7. Mitchell, R. R.; Gallant, B. M.; Thompson, C. V.; Shao-Horn, Y. All-Carbon-Nanofiber Electrodes for High-Energy Rechargeable Li−O_2 Batteries. *Energy Environ. Sci.* **2011**, *4*, 2952.
8. Lu, Y.; Kwabi, D.; Yao, K.; Harding, J. R.; Zhou, J.; Zuin, L.; Shao-Horn, Y. The Discharge Rate Capability of Rechargeable Li−O_2 Batteries. *Energy Environ. Sci.* **2011**, *4*, 2999–3007.
9. Xiao, J.; Mei, D.; Li, X.; Xu, W.; Wang, D.; Graff, G. L.; Bennett, W. D.; Nie, Z.; Saraf, L. V.; Aksay, I. A.; *et al.* Hierarchically Porous Graphene as a Lithium-Air Battery Electrode. *Nano Lett.* **2011**, *11*, 5071–5078.
10. McCloskey, B. D.; Valery, A.; Luntz, A. C.; Gowda, S. R.; Wallraff, G. M.; Garcia, J. M.; Mori, T.; Krupp, L. E. Combining Accurate O_2 and Li_2O_2 Assays to Separate Discharge and Charge Stability Limitations in Nonaqueous Li−O_2 Batteries. *J. Phys. Chem. Lett.* **2013**, *4*, 2989–2993.
11. Oh, D.; Qi, J.; Lu, Y.-C.; Zhang, Y.; Shao-Horn, Y.; Belcher, A. M. Biologically Enhanced Cathode Design for Improved Capacity and Cycle Life for Lithium-Oxygen Batteries. *Nat. Commun.* **2013**, *4*, 2756.
12. Ottakam Thotiyl, M. M.; Freunberger, S. a; Peng, Z.; Chen, Y.; Liu, Z.; Bruce, P. G. A Stable Cathode for the Aprotic Li−-O_2 Battery. *Nat. Mater.* **2013**, *12*, 1050–1056.
13. Peng, Z.; Freunberger, S.; Chen, Y.; Bruce, P. A Reversible and Higher-Rate Li−O_2 Battery. *Science* **2012**, *337*, 563–566.
14. Mitchell, R. R.; Gallant, B. M.; Thompson, C. V.; Shao-Horn, Y. All-Carbon-Nanofiber Electrodes for High-Energy Rechargeable Li−O_2 Batteries. *Energy Environ. Sci.* **2011**, *4*, 2952.
15. Wang, Z.-L.; Xu, D.; Xu, J.-J.; Zhang, L.-L.; Zhang, X.-B. Graphene Oxide Gel-Derived, Free-Standing, Hierarchically Porous Carbon for High-Capacity and High-Rate Rechargeable Li−O_2 Batteries. *Adv. Funct. Mater.* **2012**, *22*, 3699–3705.
16. Bryantsev, V. S.; Uddin, J.; Giordani, V.; Walker, W.; Addison, D.; Chase, G. V. The Identification of Stable Solvents for Nonaqueous Rechargeable Li-Air Batteries. *J. Electrochem. Soc.* **2012**, *160*, A160–A171.
17. Jung, H.-G.; Hassoun, J.; Park, J.-B.; Sun, Y.-K.; Scrosati, B. An Improved High-Performance Lithium-Air Battery. *Nat. Chem.* **2012**, *4*, 579–585.
18. Schaedler, T. A.; Jacobsen, A. J.; Torrents, A.; Sorensen, A. E.; Lian, J.; Greer, J. R.; Valdevit, L.; Carter, W. B. Ultralight Metallic Microlattices. *Science* **2011**, *334*, 962–965.
19. Maloney, K. J.; Roper, C. S.; Jacobsen, A. J.; Carter, W. B.; Valdevit, L.; Schaedler, T. A. Microlattices as Architected Thin Films: Analysis of Mechanical Properties and High Strain Elastic Recovery. *APL Mater.* **2013**, *1*, 022106.
20. Jacobsen, A. J.; Barvosa-Carter, W.; Nutt, S. Compression Behavior of Micro-Scale Truss Structures Formed from Self-Propagating Polymer Waveguides. *Acta Mater.* **2007**, *55*, 6724–6733.
21. Woods, R.; Bard, A. J. *Electroanalytical Chemistry, A Series of Advances*; Marcel Dekker: New York, 1976; Vol. 9.
22. Sarapuu, A.; Nurmik, M.; Mändar, H.; Rosental, A.; Laaksonen, T.; Kontturi, K.; Schiffrin, D. J.; Tammeveski, K. Electrochemical Reduction of Oxygen on Nanostructured Gold Electrodes. *J. Electroanal. Chem.* **2008**, *612*, 78–86.
23. Burckel, D. B.; Washburn, C. M.; Raub, A. K.; Brueck, S. R. J.; Wheeler, D. R.; Brozik, S. M.; Polsky, R. Lithographically Defined Porous Carbon Electrodes. *Small* **2009**, *5*, 2792–2796.
24. Rys, J.; Valdevit, L.; Schaedler, T. a.; Jacobsen, A. J.; Carter, W. B.; Greer, J. R. Fabrication and Deformation of Metallic Glass Micro-Lattices. *Adv. Eng. Mater.* **2014**, *16*, 889–896.
25. Gallant, B. M.; Kwabi, D. G.; Mitchell, R. R.; Zhou, J.; Thompson, C. V.; Shao-Horn, Y. Influence of Li_2O_2 Morphology on Oxygen Reduction and Evolution Kinetics in Li−O_2 Batteries. *Energy Environ. Sci.* **2013**, *6*, 2518.
26. Horstmann, B.; Gallant, B.; Mitchell, R.; Bessler, W. G.; Shao-Horn, Y.; Bazant, M. Z. Rate-Dependent Morphology of Li_2O_2 Growth in Li−O_2 Batteries. *J. Phys. Chem. Lett.* **2013**, *4*, 4217–4222.
27. Adams, B. D.; Radtke, C.; Black, R.; Trudeau, M. L.; Zaghib, K.; Nazar, L. F. Current Density Dependence of Peroxide Formation in the Li−O_2 Battery and Its Effect on Charge. *Energy Environ. Sci.* **2013**, *6*, 1772.
28. Aetukuri, N. B.; McCloskey, B. D.; García, J. M.; Krupp, L. E.; Viswanathan, V.; Luntz, A. C. Solvating Additives Drive Solution-Mediated Electrochemistry and Enhance Toroid Growth in Non-Aqueous Li−O_2 Batteries. *Nat. Chem.* **2014**, *7*, 50–56.
29. Schwenke, K. U.; Metzger, M.; Restle, T.; Piana, M.; Gasteiger, H. A. The Influence of Water and Protons on Li_2O_2 Crystal Growth in Aprotic Li−O_2 Cells. *J. Electrochem. Soc.* **2015**, *162*, A573–A584.
30. Meini, S.; Piana, M.; Beyer, H.; Schwammlein, J.; Gasteiger, H. A. Effect of Carbon Surface Area on First Discharge Capacity of Li−O_2 Cathodes and Cycle-Life Behavior in Ether-Based Electrolytes. *J. Electrochem. Soc.* **2012**, *159*, A2135–A2142.
31. Schwenke, K. U.; Meini, S.; Wu, X.; Gasteiger, H. a; Piana, M. Stability of Superoxide Radicals in Glyme Solvents for Non-Aqueous Li−O_2 Battery Electrolytes. *Phys. Chem. Chem. Phys.* **2013**, *15*, 11830–11839.
32. Meini, S.; Piana, M.; Tsiouvaras, N.; Garsuch, A.; Gasteiger, H. A. The Effect of Water on the Discharge Capacity of a Non-Catalyzed Carbon Cathode for Li−O_2 Batteries. *Electrochem. Solid-State Lett.* **2012**, *15*, A45.
33. Nakamoto, K. *Infrared and Raman Spectra of Inorganic and Coordination Compounds: Part B: Applications in Coordination, Organometallic, and Bioinorganic Chemistry*; John Wiley and Sons: New York, 2008.
34. Siebert, F.; Hildebrandt, P. *Vibrational Spectroscopy in Life Science*; Wiley-VCH Verlag GmbH & Co. KGaA: Weinheim, 2008.
35. Vijh, A.; Kim, C.; Cho, M. H.; Trottier, J.; Gagnon, C.; Hovington, P.; Cl, D.; Guer, A.; Black, R.; Nazar, L.; *et al.* The Effects of Moisture Contamination in the Li−O_2 Battery. *J. Power Sources* **2014**, *268*, 2–11.
36. Black, R.; Oh, S. H.; Lee, J.-H.; Yim, T.; Adams, B.; Nazar, L. F. Screening for Superoxide Reactivity in Li−O_2 Batteries: Effect on Li_2O_2/LiOH Crystallization. *J. Am. Chem. Soc.* **2012**, *134*, 2902–2905.
37. Sharon, D.; Afri, M.; Noked, M.; Garsuch, A.; Frimer, A. A.; Aurbach, D. Oxidation of Dimethyl Sulfoxide Solutions by Electrochemical Reduction of Oxygen. *J. Phys. Chem. Lett.* **2013**, *4*, 3115–3119.

38. Zakharchenko, T. K.; Kozmenkova, A. Y.; Itkis, D. M.; Goodilin, E. A. Lithium Peroxide Crystal Clusters as a Natural Growth Feature of Discharge Products in Li−O_2 Cells. *Beilstein J. Nanotechnol.* **2013**, *4*, 758–762.
39. Song, K.; Jung, J.; Heo, Y.-U.; Lee, Y. C.; Cho, K.; Kang, Y.-M. A-MnO_2 Nanowire Catalysts with Ultra-High Capacity and Extremely Low Overpotential in Lithium-Air Batteries through Tailored Surface Arrangement. *Phys. Chem. Chem. Phys.* **2013**, *15*, 20075–20079.
40. Liu, W.-M.; Gao, T.-T.; Yang, Y.; Sun, Q.; Fu, Z.-W. A Hierarchical Three-Dimensional $NiCo_2O_4$ Nanowire Array/carbon Cloth as an Air Electrode for Nonaqueous Li-Air Batteries. *Phys. Chem. Chem. Phys.* **2013**, *15*, 15806–15810.
41. Montemayor, L. C.; Meza, L. R.; Greer, J. R. Design and Fabrication of Hollow Rigid Nanolattices *via* Two-Photon Lithography. *Adv. Eng. Mater.* **2014**, *16*, 184–189.
42. Sattayasamitsathit, S.; O'Mahony, A. M.; Xiao, X.; Brozik, S. M.; Washburn, C. M.; Wheeler, D. R.; Gao, W.; Minteer, S.; Cha, J.; Burckel, D. B.; *et al.* Highly Ordered Tailored Three-Dimensional Hierarchical Nano/microporous Gold−Carbon Architectures. *J. Mater. Chem.* **2012**, *22*, 11950.
43. Zhang, H.; Yu, X.; Braun, P. V. Three-Dimensional Bicontinuous Ultrafast-Charge and -Discharge Bulk Battery Electrodes. *Nat. Nanotechnol.* **2011**, *6*, 277–281.
44. Zheng, X.; Lee, H.; Weisgraber, T. H.; Shusteff, M.; DeOtte, J.; Duoss, E. B.; Kuntz, J. D.; Biener, M. M.; Ge, Q.; Jackson, J. A.; *et al.* Ultralight, Ultrastiff Mechanical Metamaterials. *Science* **2014**, *344*, 1373–1377.